J Appl Electrochem (2010) 40:757–765
DOI 10.1007/s10800-009-0054-5

ORIGINAL PAPER

Electrochemical methods to analyse the light-induced plating process

J. Bartsch · V. Radtke · C. Schetter · S. W. Glunz

Received: 2 July 2009 / Accepted: 1 December 2009 / Published online: 15 December 2009

Abstract This study deals with some specific characteristics that the light-induced plating (LIP) process, which is used for the metallisation of solar cells, exhibits compared to classical electroplating processes. We contribute to the general understanding of LIP (multiple electrodes, influence of light) with some basic experiments and propose a simplified equivalent circuit scheme. We also address the challenge of process control through potential and current without external connection of the working electrode (front side grid). In this article, we show a possibility to determine the absolute potential of the front side grid for relevant process parameters. Furthermore, we present a method that allows the measurement of the mean current density at the front side grid during the process, which has a great influence on the plating result.

Keywords Crystalline solar cells · Light-induced plating · Absolute potential measurement · Current density

1 Introduction

Classical electrochemical metal-plating processes are realised by immersing the workpiece that is meant to be electroplated into a suitable electrolyte and setting this workpiece to a cathodic (negative) potential against an anode (mostly made of the plated material). The process control is realised monitoring several parameters. Two very important ones are the current density at the workpiece surface and its absolute potential (against the Normal Hydrogen Electrode, NHE). Both are easily accessible, the first by measuring the current that goes through the outer circuit (which must also be the current through the workpiece), the second using a reference electrode.

The situation is very different for the light-induced plating (LIP) process. This technique, which was first described in 1975 [8], can be used for the electrodeposition on semiconductors with a p–n-junction. It utilises their photovoltaic effect to induce a voltage between p- and n-area under irradiation without any need for external contacting of the front side grid. While this is a huge advantage regarding process simplification, the above-mentioned important parameters become inaccessible as there is no external circuit.

Interest for LIP is renewed as it is suitable for advanced metallisation techniques of solar cells. It has been long used for the front side metallisation of laboratory high-efficiency cell structures, proving the potential of this technique. Moreover, efficiency gains of a two-step metallisation concept (seed-layer + LIP, as described in [4]) compared to cells with standard metallisation (screen printing and firing of metal pastes) have been shown on an industrial scale (e.g. [1, 3]). LIP is especially beneficial for solar cells, since the demanding contacting of the very narrow lines of the front side becomes needless. On the other hand, the fully metallised, p-doped rear side is easy to contact. This needs to be done to protect it against anodic processes if the cell is fully immersed into the electrolyte. For this, a protective potential $\Delta E_{\mathrm{RS\text{-}AUX}}$ is applied between the rear side and an auxiliary electrode of the metal that is meant to be plated. Figure 1 shows the working principle of LIP.

Current and voltage that can be measured in the outer circuit of this setup only represent processes between rear side and anode. However, the front side is of a greater

J. Bartsch (✉) · V. Radtke · C. Schetter · S. W. Glunz
Fraunhofer ISE, Heidenhofstr. 2, 79110 Freiburg, Germany
e-mail: jonas.bartsch@ise.fraunhofer.de

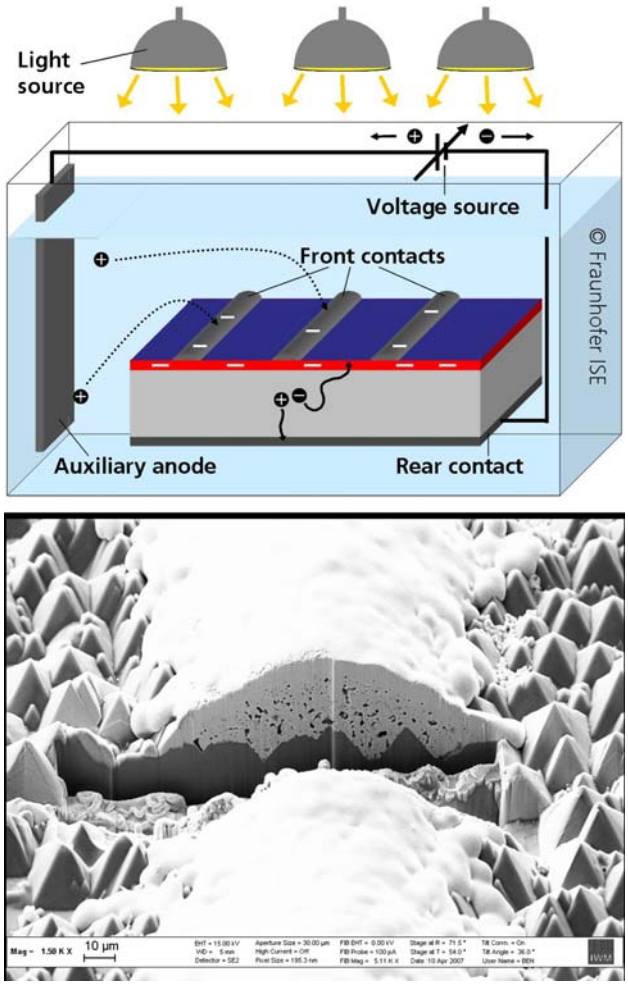

Fig. 1 *Upper picture* Schematic illustration of the working principle of LIP. *Lower picture* SEM-Image of a cross section (prepared with the FIB-method) of a screen printed and silver plated solar cell contact. The highly conductive, dense layer applied by LIP is clearly visible upon the porous screen printed seed layer [7]

interest, as the deposition that occurs there defines the properties of the resulting solar cell contacts (e.g. specific conductivity, aspect ratio). These processes are not directly accessible, as a direct current measurement at the front side interferes with the process. The investigations presented here show a solution to this problem, enabling a better understanding of the front side deposition process.

2 Experimental

For the plating experiments, solar cell test structures were designed specifically. We used monocrystalline 156 × 156 mm^2 preprocessed substrates from a typical industrial production to guarantee reproducible substrate properties. These substrates had already received random pyramid texture, an emitter diffusion (50 $\Omega\ sq^{-1}$), plasma edge isolation and a PECVD SiN_x ARC. We applied a full rear side metallisation with a standard aluminium-paste screen-print process. The front side metallisation was applied either with a standard screen-printing process or with an aerosol-jetting process [6]. The printing pattern was chosen to give 50 × 50 mm^2 cells with two busbars of 1 mm width at the cell edges, to facilitate resistance measurements. The resulting front side metallisation was characterised comprehensively before the plating step, to evaluate the total metal-surface area of the solar cell grid. The cell-structures were separated with a dicing saw (Disco). Where edges and/or surfaces of these cells needed to be protected against processes, it was done with Zuelch OSTROLUX protective resist, which is stable against the chemicals of the electrolyte.

All experiments were carried out in an experimental setup as schematically shown in Fig. 2. In a container, solar cells or other substrates like disc electrodes can be immersed into an electrolyte and set to defined potentials versus counter or reference electrodes with a multipotentiostat. For illumination of the solar cells, the container features a window at one side. Different light sources can be used for irradiation, among these LED arrays. The current source used for the light is controlled with a function generator. The electrolyte is circulated through the setup by a pump through a filter (1 µm), the flow can be adjusted with a choke valve and monitored by a flowmeter. It is being led back into the container through a distribution pipe, allowing an adjustment of the direction of flow. The temperature of the electrolyte is automatically regulated by a heating. The used electrolyte was a commercially available non-cyanidic silver solution. Temperature and electrolyte properties were kept constant between all experiments and according to the manufacturers' specifications. Potentials and currents were applied and measured using a VSP-multipotentiostat (Bio-Logic).

For the potential measurements, the rim of one screen-printed cell was protected with resist, to prevent shunting through metal growth over the rim. This cell was put into a standard process setup, using one channel of the potentiostat to apply a potential between rear side (working electrode, WE) and auxiliary anode (counter and reference electrode, CE and REF). On a second, synchronised channel, all electrodes were additionally operated as WE against a reference ($Hg/Hg_2SO_4/K_2SO_4$ sat., Radiometer Analytical) as REF alternately, with a platinum sheet as CE.

For current density experiments, the cells were weighed with a laboratory balance (Sartorius) before plating, then the rear side was coated with resist. A small rim of the rear side was left uncovered for contacting of the cells. During the experiment, this uncovered rim was left out of the electrolyte. The edges of the cells were also covered with resist to rule out shunting effects. The resist was dried overnight, and the cells were weighed again afterwards.

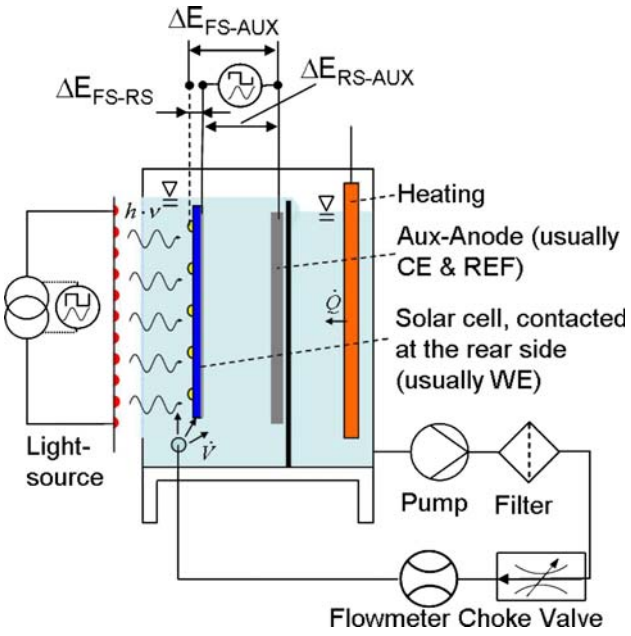

Fig. 2 Schematic picture of the used manual plating setup

They were then plated in the manual plating setup described above. Light intensity and rear side potential were adjusted with the current/voltage sources. Thus, also the current density was altered. The plating time was chosen for each set of parameters to give comparable deposition masses.

After plating, the cells were rinsed with deionised water, dried and weighed. The resist was stripped off with acetone, the cells were dried and weighed again. If the difference of weight gain between the two measurements was too high, the experiment was repeated with a new cell. The plated surface was estimated using the substrate properties known from the evaluation, and the mean current density was calculated as described below.

3 Results

The major process parameters influencing the electrodeposition of metals are the absolute overpotential of the workpiece used for the deposition η and the surface concentration of the electroactive species c^s in front of the workpiece. The former can be adjusted directly, the latter indirectly in a process. This is crucial to deposit a metal layer of high quality, exhibiting the desired properties (e.g. high conductivity).

Two other very important parameters are the substrate geometry and the used electrolyte system. However, changing them usually means changing the process fundamentally, which requires considerable efforts. We will, therefore, focus on the two before-mentioned parameters. The absolute overpotential influences the rate of the charge transfer step of the reaction, as it can alter the intrinsic energy level of the reactants in the vicinity of the electrode. The reactants are activated, so the activation barrier for charge transfer can be overcome more easily. For a cathodic process, this is expressed by the following correlations:

$$\Delta G_c^{\neq}(E_2) = \Delta G_c^{\neq}(E_1) + (1-\alpha)nF\Delta E \tag{1}$$

describes the change in Gibbs free energy ($\Delta G_c{}^{\neq}(E)$) or activation energy needed for the cathodic charge transfer reaction, in dependence of the cathode potential E. F is the faraday constant, n the stoichiometric number of electrons for the reduction and α is the transfer coefficient (between zero and unity). With the cathodic reaction rate being

$$J_c = k_c^0 c_{ox}^s exp\left[-\frac{\Delta G_c^{\neq}(E)}{RT}\right], \tag{2}$$

one can see the important influence of the cathode potential in the numerator of the exponential term (k_c^0 is the rate coefficient for the cathodic reaction, c_{ox}^s is the surface concentration of the electroactive cation).

With the overpotential η as degree for the potentials displacement from equilibrium:

$$\eta = E - E_{eq} \tag{3}$$

and the exchange current density j_0 for the cathode

$$j_{0c} = nFc_{ox}^s k_0^{'c} e^{-\frac{\Delta G_c^{\neq}(E_{eq})}{RT}} \tag{4}$$

the cathodic charge transfer current density can be written as

$$j_D^-(E) = -j_{0c} exp\left[-\frac{(1-\alpha)nF}{RT}\eta_{ct}\right] \tag{5}$$

where η_{ct} is the charge transfer overpotential [2, 5].

The charge transfer step should always be the rate limiting step of the reaction chain, to prevent a complete depletion of the reactants at the electrode surface. However, as the process should be as fast as possible, it is desirable to improve the mass transfer to the surface rather than slowing down the charge transfer rate. The latter should then be kept just below the mass transfer rate, which will lead to an acceptable surface concentration of the reactants. The surface concentration, on the other hand, can also be altered, by adjusting the bulk concentration of the electroactive species and the width of the diffusion layer (through forced convection).

Of course, the flux of the electroactive species is proportional to the surface area of the substrate (the unit of the flux is mol m^{-2} s^{-1}). At a constant current, the surface concentration will increase proportionally to the surface area. In order to detach considerations from the latter, the current density is usually used.

Even more significant is the limiting current density, which also takes into account the former two aspects (bulk concentration, convection) for a given system, thus showing its limitations. While overpotential and current density are easily accessible for classical electrochemical reactions, this is not the case for LIP. The process situation in general is very different for LIP, complicating a description. In total, three electrodes need to be considered: The front side grid (FS), which is meant to be the workpiece of the process, the rear side (RS), where a potential is applied to protect it against dissolution, but also to influence the front side potential, and the auxiliary anode (AUX), to where the anodic process is shifted. Furthermore, the workpiece is also a current source (under irradiation), which makes a description even more demanding. The front side grid is not connected directly to any outer circuit during the process, thus there is no direct access to any parameters that settle there.

3.1 Evaluation of the general behaviour of LIP

In order to understand the behaviour of all electrodes and current paths in the LIP-process, we investigated them separately in several experiments (Fig. 3a–e). First, we used only solar cells, without connecting an anode. A solar cell with a covered rear side was introduced into the electrolyte and irradiated (Fig. 3a). As no anodic counter process could occur, there was no silver deposition to the front side grid. This is different for a solar cell without rear side protection (Fig. 3b), where silver is deposited onto the front side. This shows the behaviour of the solar cell as a short-circuited current source in the electrolyte. The corresponding anodic process is the dissolution of the rear side aluminium.

Then, the auxiliary anode was introduced into the system, first regarding only the front side in addition, again using a cell with a covered rear side. The cell was not completely introduced into the electrolyte, and a small rim above the fluid level was left uncovered, to connect the rear side to the anode analogous to the process (Fig. 3c). The cell was irradiated, but no potential between rear side and anode was applied. Nevertheless, deposition of silver to the front side could be observed with the light microscope. The current between rear side and anode (I_{LIP}) and the deposited mass could be increased (Fig. 4) by applying and increasing a protective potential $\Delta E_{RS\text{-}AUX}$ between rear side and anode (Fig. 3d). This is due to the front side potential following $\Delta E_{RS\text{-}AUX}$, a behaviour that is observable under irradiation as can be seen in Fig. 5.

When additionally introducing the rear side into the system (giving the original process, (Fig. 3e), silver deposition (or alumina dissolution) can be found there too, depending on the applied $\Delta E_{RS\text{-}AUX}$ and the irradiation

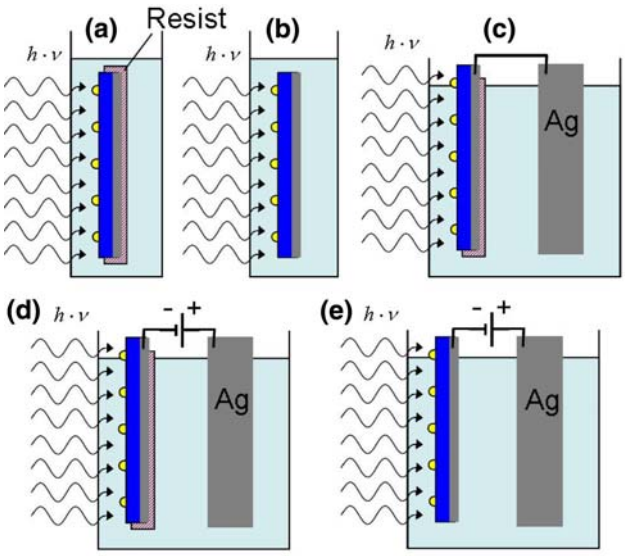

Fig. 3 Different experimental setups used to determine all possible current paths in the LIP process. In setup a, no processes occur. In setup b, silver is deposited to the front side grid while the rear side dissolves. For setups c and d, the anode is dissolved and silver is deposited to the front side grid. In setup e, silver is plated to the front side while either the rear side or the anode (depending on the applied potential) are dissolved

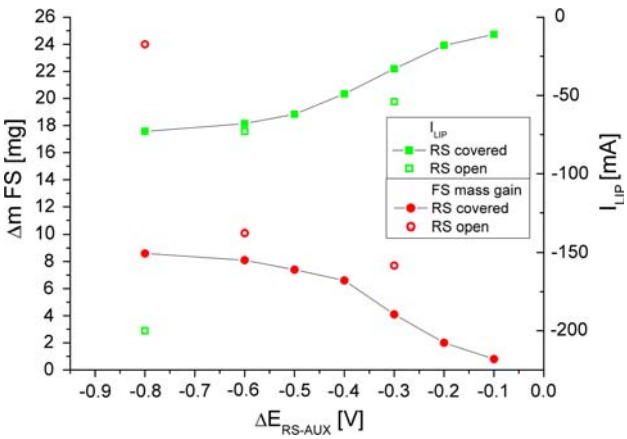

Fig. 4 Weight gain of a cell that was plated at different potentials between rear side and anode with a protected rear side, with a deposition time of 2 min for each potential. The hollow symbols show the results for measurements at the same parameters (50 W irradiation) with separated FS and RS electrodes as described below

intensity. After long plating times at suitable protective potentials, a clearly visible silver layer shows at the rear side. This is favourable to dissolution of the alumina rear side, which will contaminate the electrolyte if the absolute potential is chosen too low.

From these experiments, we derived a simplified equivalent circuit diagram of the system (disregarding the electrode surface behaviour as resistor/capacitance), which is shown in Fig. 6. Instead of only one current path (such as

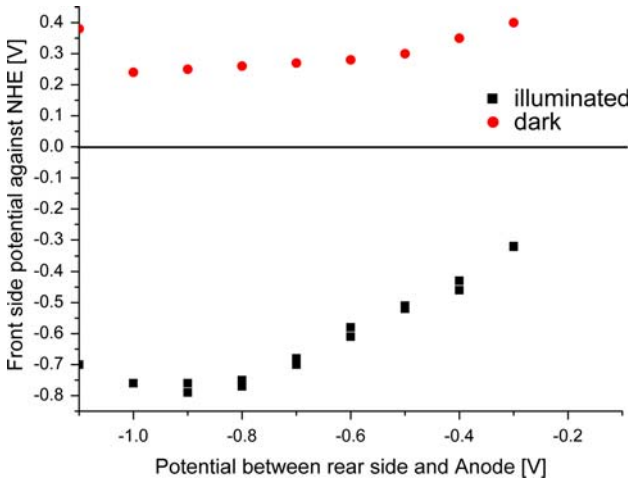

Fig. 5 Absolute potential of the front side in the dark/at constant illumination in dependence of $\Delta E_{\text{RS-AUX}}$

in a conventional electroplating process), the system consists of three current circuits. Table 1 lists all circuits and the corresponding electrodes. It becomes clear that the rear side has an anodic function in circuit 3, while it has a cathodic function (depending on the protective potential) in circuit 1. As circuit 3 can be interpreted as a solar cell short circuited by the electrolyte, all electrode potentials and currents depend on the working point of the solar cell at the process parameters. These issues will be addressed in the following.

The influence of the solar cell working point at given process parameters has been reported before [7]. When altering the irradiance and $\Delta E_{\text{RS-AUX}}$, the current measured between the rear side and the anode plotted against the potential between rear and front side is found to mirror the I–V-curve of a solar cell. If the part of the rear side which is in contact with the electrolyte is protected with a resist, the curve resembles an I−V-curve with high series resistance, which is due to the resistance of the electrolyte and of the transfer reactions. On this basis, we modified the experiment to model the LIP process by using not covered solar cells. Figure 7 shows the resulting curves for four different irradiation powers. The formerly reported results

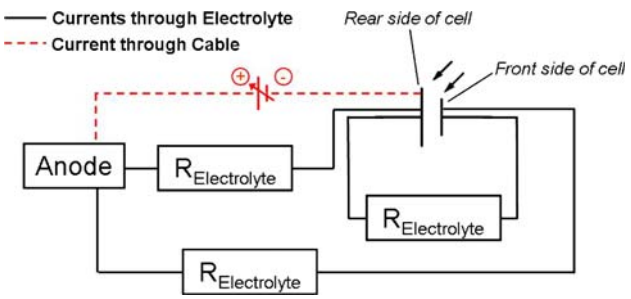

Fig. 6 Simplified equivalent circuit scheme for the LIP-Process

Table 1 Circuits of the system LIP for values of $\Delta E_{\text{RS-AUX}}$ and irradiation intensity usually chosen for a process. Depending on these parameters, the direction of the circuits may change (see below)

Circuit	Description	Anode	Cathode
1	Protective potential	AUX	RS
2	Direct deposition	AUX	FS
3	Solar cell short circuit	RS	FS

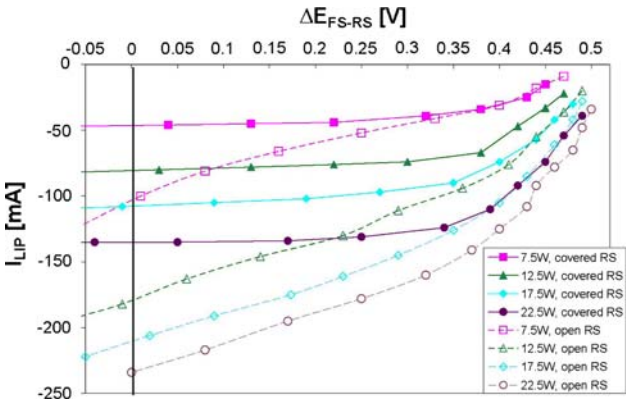

Fig. 7 Behaviour of solar cells with covered (*full symbols*) and open (*hollow symbols*) rear side for $\Delta E_{\text{RS-AUX}}$ varied from −0.2 to −1.4 V in steps of 0.1 V and different irradiation intensities

could be reproduced very well. I–V-curves of cells with an open rear side show a shunt characteristic additionally, the cell is shunted by the electrolyte. The experiment makes clear that the current I_{LIP}, which is measured between rear side and anode, is not necessarily the same as over the front side grid. The current measured with the additional presence of a rear side is higher if the potential $\Delta E_{\text{RS-AUX}}$ applied is high enough. This is due to the processes that occur at the rear side, which has a large metal surface area (approx. ten times larger than the front side). These can only occur if the RS is in contact to the electrolyte. A more detailed analysis of this behaviour is given below.

3.2 Absolute overpotential of the front side grid

The essential parameter for the LIP-process is the potential at the front side grid E_{FS}. With the described dependence of irradiance and protective potential, we chose to measure the potential of the front side grid against a reference electrode, taking data points for conventional sets of these parameters. Furthermore, we also measured the absolute potentials for both other electrodes, and all relative potentials for the same process parameters, to validate our measurements. From this evaluation, we could derive 3-D contour-plots of the absolute potentials against NHE for all electrodes in the process. Figure 8 shows the front side grid potential. The same kind of graph results for the rear side

and the auxiliary anode (not shown). As can be seen, the absolute potential at the front side grid E_{FS} decreases for increasing light intensity and decreasing $\Delta E_{RS\text{-}AUX}$.

For the validation of the measurements, we compared the differences of the absolute potentials to the measured relative potentials between all electrodes. The following equations should be fulfilled:

$$E_{FS,abs} - E_{RS,abs} = \Delta E_{FS-RS} \quad (6)$$

$$E_{FS,abs} - E_{AUX,abs} = \Delta E_{FS-AUX} \quad (7)$$

$$E_{RS,abs} - E_{AUX,abs} = \Delta E_{RS-AUX} \quad (8)$$

Therefore, subtracting the relative potentials from the difference of absolute potentials should give a value close to zero for a valid measurement. We found this condition to be fulfilled for all values except for parameters pairs where $\Delta E_{RS\text{-}AUX}$ was very high and the illumination was very low. At these working points, we are in a region of the I–V-curve where the solar cell potential changes very quickly, and so already a slight change in the experimental setup may cause important changes (see Fig. 9). As all relative and absolute potentials are measured in independent experiments, the working point that settles may slightly differ for each one which has most impact for the points highlighted in Fig. 9. We are currently improving our setup to be able to measure all absolute potentials at the same time. We can then check whether we can get consistent results for all sets of parameters, or if the described behaviour is caused by some other effect we do not understand yet. For most of the values, however, the deviance from the optimal 'mathematical' behaviour as described in Eqs. 6–8 was found to be less than 5% (Fig. 10).

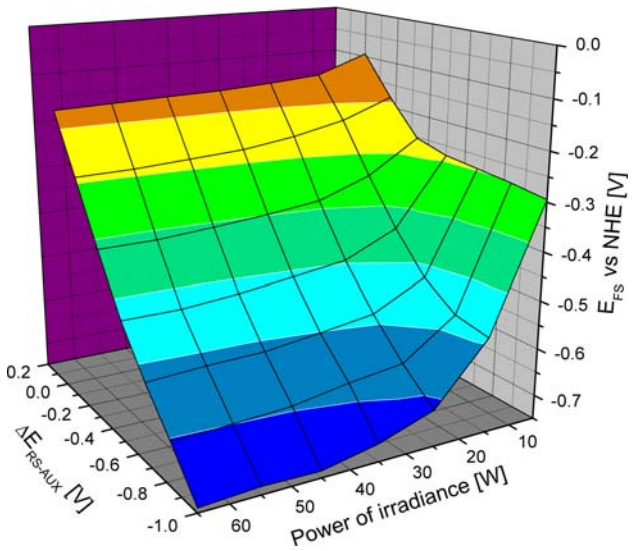

Fig. 8 Absolute potential of the front side grid against NHE for the relevant process parameters

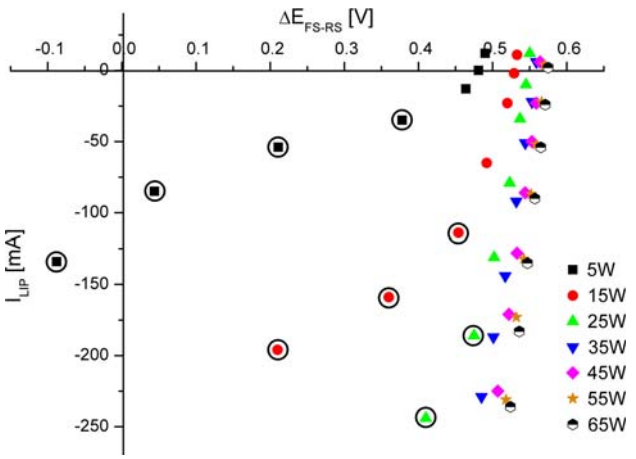

Fig. 9 I–V-curves that were taken during one of the potential measurements. The circled spots indicate parameter sets with a relatively high deviation, which occurs in a region of the curve where the potential changes rapidly

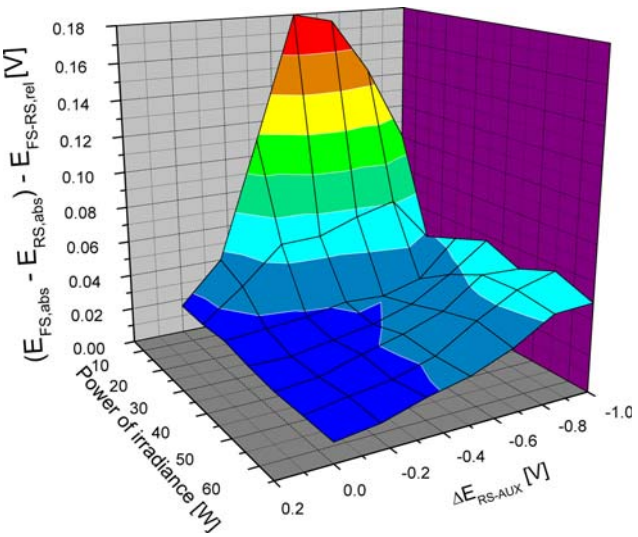

Fig. 10 Deviation of the absolute Potentials compared to the relative measured potentials between the different measurements. For most values, good agreement with Eq. 6 was found

As mentioned before, the results shown here are only valid for the considered cell, as they depend on its I–V characteristic. Also, they are only valid for experimental setups with comparable conditions. Especially, the irradiance may alter considerably with only slight changes in the setup. Nevertheless, the *method* presented here will be of great value. In industrial production lines, the performance of all cells ought to be in a quite narrow margin. Also, the plating device is always the same. The experiment could be done with a typical cell, at the conditions of the process (preferably in the inline-device itself), giving a good knowledge of the front side behaviour and allowing a process optimisation. Additional voltammetric experiments

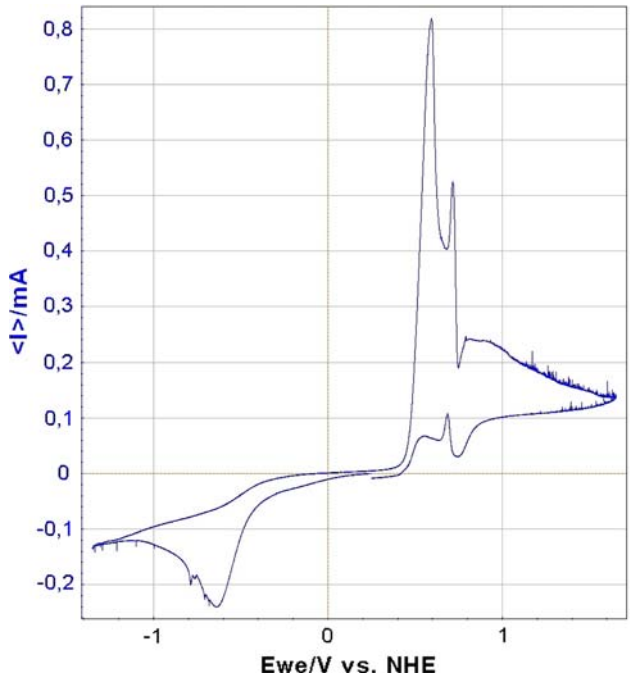

Fig. 11 Cyclic voltammogram of the used electrolyte with a silver disc electrode as WE, a platinum sheet as CE and a $Hg/Hg_2SO_4/K_2SO_4$ sat. electrode as REF, at 100 mV s^{-1} sweep rate. The cathodic branch shows silver deposition at very different rates for potentials lower than 200 mV versus NHE

allow an analysis of the deposition behaviour of the electrolyte system (Fig. 11). The front side potential can then be set to a point where deposition rate and quality give the best compromise.

3.3 Method for measuring the mean current density

As mentioned above, a measurement of the current and consequently the current density over the front side electrode cannot be done directly. The current meter would interfere with the process, and the obtained value would not represent the current during the process. Also, the conventional method of weighing is not possible, as processes at the rear side also alter the weight of the cell, so the mass gain will not result from the front side exclusively. If the rear side is covered, e.g. with a resist, to avoid this problem, all processes occur at the front side and the mean current density can be obtained. However, as this setup does not represent the original LIP process (compare Fig. 7), it is not suited to give the desired information.

In order to solve this inaccuracy, we introduced two cells into the electrolyte, one with a covered front side and one with a covered rear side. The resist used for the covering was completely impermeable for light. The rear sides of both cells were connected to have them adopt the same potential. The potential $\Delta E_{\text{RS-AUX}}$ was now applied between both rear sides and the anode. This experimental

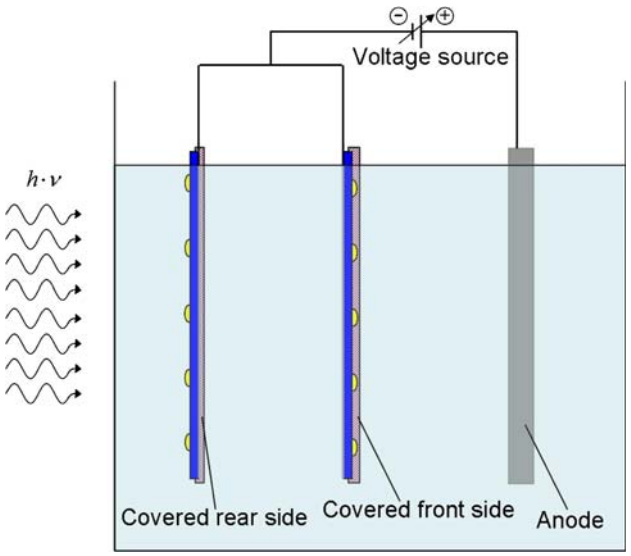

Fig. 12 Schematic picture of the experimental setup used to measure averaged current densities

setup virtually separates all the electrodes and still mirrors the situation during the original process. Most currents are accessible not directly, but through weight measurements. A schematic picture of the resulting setup is shown in Fig. 12. In order to confirm the correct reproduction of the original system, we measured the absolute potentials of all electrodes in both the original setup and the setup with 'isolated electrodes' against a reference electrode as described above. The found values were perfectly comparable within the usual experimental deviation (10 mV). Therefore, in this setup, all the electrodes behave exactly as they do in the original process. The average current over the electrodes can be determined by measuring the weight gain per time of each separated electrode. The total current during the process can then be calculated with Faraday's law (assuming a current efficiency close to one):

$$Q = \frac{m * z * F}{M} \tag{9}$$

and the correlation between mean current and charge:

$$\bar{I} = \frac{Q}{t}. \tag{10}$$

Repeating the experiment described in Fig. 4 with this new setup, the difference made by the rear side shows clearly. In the measurement that was done with a protected rear side, the current I_{LIP} and the deposited silver mass were a lot lower that in the one with an additional rear side. This is easily explicable, as the current measured in the first setup can only be the current that is delivered by the solar cell. While the voltage source may apply a potential between rear side and anode, it cannot induce a current flow, as the rear side is not in contact with the electrolyte and the current circuit is interrupted. Thus, the current is

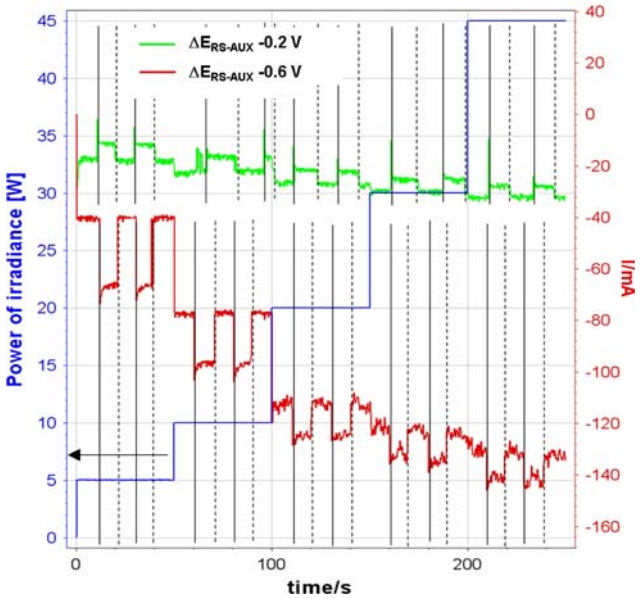

Fig. 13 Current over the auxiliary anode measured in experiment where an isolated rear side was connected (*solid vertical lines*) and disconnected (*dashed vertical lines*) to the system. Measurements for two values $\Delta E_{\text{RS-AUX}}$ (−0.2 V, −0.6 V) and different irradiation intensities

higher for the setup with an additional rear side, especially for high absolute potentials, which is in good agreement with the I–V-curves measured with an open rear side (Fig. 7). Under these conditions, the deposition of silver to the rear side becomes significant. This behaviour was confirmed in another experiment regarding the influence of the additional 'isolated rear side'. The process was started without the uncovered rear side connected to the system. When it was connected after several seconds, the measured current I_{LIP} changed, depending on the applied $\Delta E_{\text{RS-AUX}}$ and the irradiance (Fig. 13). For very negative values of $\Delta E_{\text{RS-AUX}}$, we measured again an increasing current. For relatively low absolute protective potentials, however, the absolute current is reduced with the introduction of the rear side which can also be seen for the points of the I–V curves with comparable potentials. We believe this to be caused by beginning anodic processes at the rear side at such potentials. The rear side potential E_{RS} is $\approx +0.2$ versus NHE under such conditions. Anodic processes at such a potential are in good agreement with the cyclic voltammogram shown in Fig. 11. We confirmed the dissolution of the rear side by separately measuring its weight difference at these parameter sets as described. This was also only possible using the new setup.

With this new technique, calculation of the mean current density and adjustment to the requirements of the LIP process for the metallisation of solar cells is possible. By estimating the total area of the plated front grid and measuring the weight gain over the process, we could

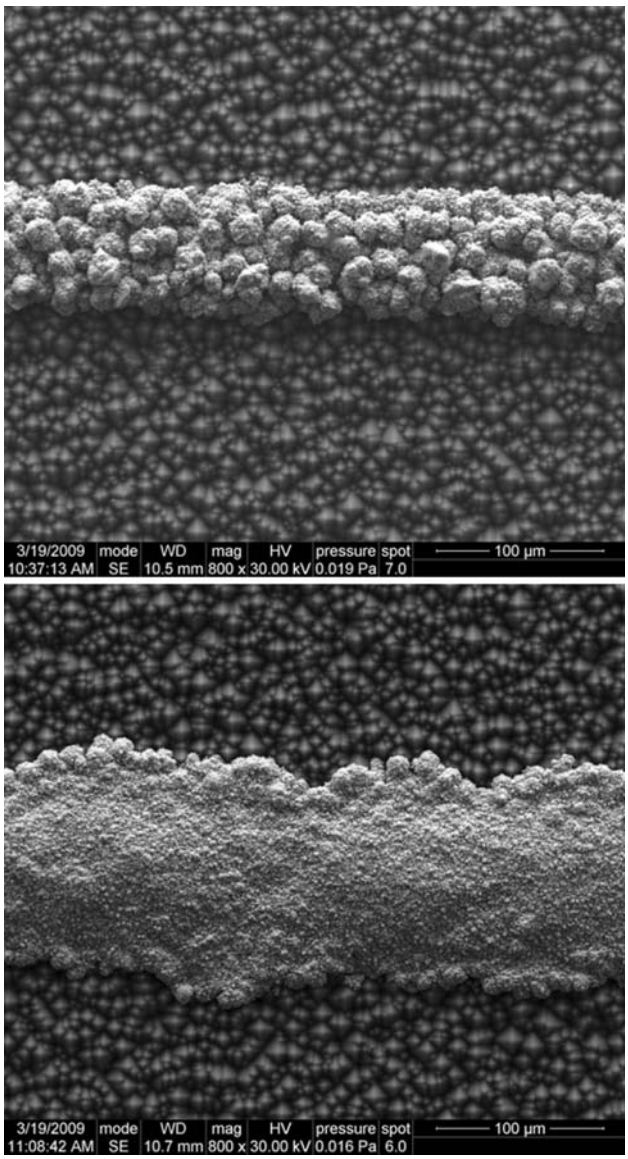

Fig. 14 SEM-Images of two solar cell contacts, plated for the same time at the same conditions (−0.4 V protective potential, same irradiation). The upper image shows an aerosol-printed contact, the mean current density was determined to be approx. 4.5 A dm^{-2}. The lower image shows a screen-printed contact, the mean current density was determined to be approx. 2.7 A dm^{-2}

determine the mean current density at the front side grid for several experiments. We already observed an influence of the width of the front side contacts to the current density. This influence may become important as the recent efforts in this area are in the direction of producing narrower contacts to increase the cell current. As the current generated by these cells is comparable or even higher than for cells with broader contacts, the current density increases rapidly with the reduction of the seed layer width. Comparing a cell with screen printed contacts (width approx. 110 µm) and one with aerosol printed contacts (width

approx. 40 μm), we found the current density to be 1.66 times higher for the latter, at the same process conditions. Also, the deposition quality is questionable for the higher current density, as can be seen in the SEM images in Fig. 14. A comprehensive, quantitative study of this behaviour, taking into account several contact properties, is currently under preparation.

4 Conclusion

In order to contribute to a better understanding of the light-induced plating (LIP)-process, we firstly examined the behaviour of the system in a few simple experiments. The influence of $\Delta E_{\mathrm{RS\text{-}AUX}}$ on the absolute potential of the front side grid E_{FS} was shown. The behaviour of all electrodes at different conditions was evaluated, and a simplified equivalent circuit is proposed based on the results. In order to be able to investigate the processes at each electrode separately, we developed an experimental setup that spatially separates the solar cell rear side from the front side without altering the system in regards to its electrochemical behaviour. Thus, we could show the solar cell to exhibit a shunted IV-characteristic in the original process setup, caused by the electrical connection between rear side and front side through the electrolyte. If the rear side is isolated from the electrolyte, the system shows a non-shunted IV-characteristic. The improved understanding and the new method for separate consideration of the electrodes enable improved techniques for process control. We showed that a mapping of the absolute front grid potential and the measurement of the current density for process parameters of interest can make an important contribution to a reliable metal deposition of good properties, most importantly if the seed layer is altered. For industrial inline-processes, which are rarely changed, the effort is very small compared to the possible benefit.

Acknowledgements The authors would like to thank Daniel Schmidt for the preparation of aerosol-printed samples and Jan Specht for the screen printing. Many thanks to Julia Pedroni for microscope measurements, potential measurements, preparation of samples etc.

References

1. Allardyce G, Cahalen J, Rasch J, Ridler T, Weigel O, Fröhlich H, Kappler H, Oberholtzer F, Rattey C, Mette A, Schetter C, Glunz SW (2007) The commercial application of light induced electroplating for improving the efficiency of crystalline silicon solar cells. In: Proceedings of the 22nd EU-PVSEC
2. Bard AJ, Faulkner LR (2001) Electrochemical methods, fundamentals and applications, 2nd edn. Wiley, New York
3. Fioramonti A (2009) Cell efficiency increase of 0.4% through light-induced plating. Photovolt Int 2:60–63
4. Glunz SW (2008) Progress in advanced metallization technology at fraunhofer ise. In: Proceedings of the 33rd IEEE photovoltaic specialists conference
5. Hamann CH, Vielstich W (1998) Elektrochemie, 3rd edn. Wiley, New York
6. Hoerteis M, Mette A, Richter P, Fidorra F, Glunz SW (2007) Further progress in metal-aerosoljet printing for front side metallization of silicon solar cells. In: Proceedings of the 22nd EU-PVSEC
7. Mette A (2007) New concepts for the front side metallization of industrial silicon solar cells. Ph.D Thesis, Albert-Ludwigs-Universität, Freiburg
8. Späth W (1975) Verfahren zur galvanischen abscheidung einer metallschicht auf der oberfläche eines halbleiterkörpers. Deutsche Patentschrift 23: 48-182